We are IntechOpen, the world's leading publisher of Open Access books Built by scientists, for scientists

4,800
Open access books available

122,000
International authors and editors

135M
Downloads

Our authors are among the

154
Countries delivered to

TOP 1%
most cited scientists

12.2%
Contributors from top 500 universities

CLARIVATE ANALYTICS BOOK CITATION INDEX INDEXED

WEB OF SCIENCE™

Selection of our books indexed in the Book Citation Index in Web of Science™ Core Collection (BKCI)

Interested in publishing with us?
Contact book.department@intechopen.com

Numbers displayed above are based on latest data collected.
For more information visit www.intechopen.com

Chapter 5

Dynamic and Quasi-Static Simulation of a Novel Compliant MEMS Force Amplifier by Matlab/Simulink

Ergin Kosa, Levent Trabzon, Umit Sonmez and Huseyin Kizil

Additional information is available at the end of the chapter

http://dx.doi.org/10.5772/46450

1. Introduction

MEMS are micro electromechanical systems having component sizes varying from 1 micrometer to 1 millimeter and provide specific engineering operations. MEMS are used as a micro sensor, micro actuator, micro accelerometer etc. and also have tendency to function rapidly due to having low inertia moment and affected less by disturbances coming from environment due to their small size (Hsu, 2002).

Compliant mechanisms having an ability to transmit motion and energy via their flexible hinges and/or flexible components instead of joints and rigid components, perform large deflections (Sreekumar et al, 2008). The large deflections of compliant mechanisms instead of rigid-body mechanisms depend on applied force that causes a much more complexity to nonlinear analysis (Ashok, 2000). Moreover, the geometry of several flexure hinges are modeled as torsion springs in its pseudo-rigid-body mechanisms (Howell, 2001). Flexible segments of compliant mechanism store and transfer energy when it is functioning (Howell, 2001; Tantanawat & S. Kota, 2007). Flexible links having small cross sections instead of traditional joints provide acting of mechanism due to its very low moment of inertia (Howell, 2001; Lobontiu et al, 2001).

Compliant four-link mechanism is designed as seen in Fig. 1 achieving force or displacement application according to the output spring constant and also, studied on size optimization to achieve maximum mechanical or geometric benefit at specific spring constants (Parkinson et al, 2001). Large displacement amplifier integrated with comb drive achieves 100 times amplifying of comb drive displacement by means of its design is modeled (Li et al, 2005).

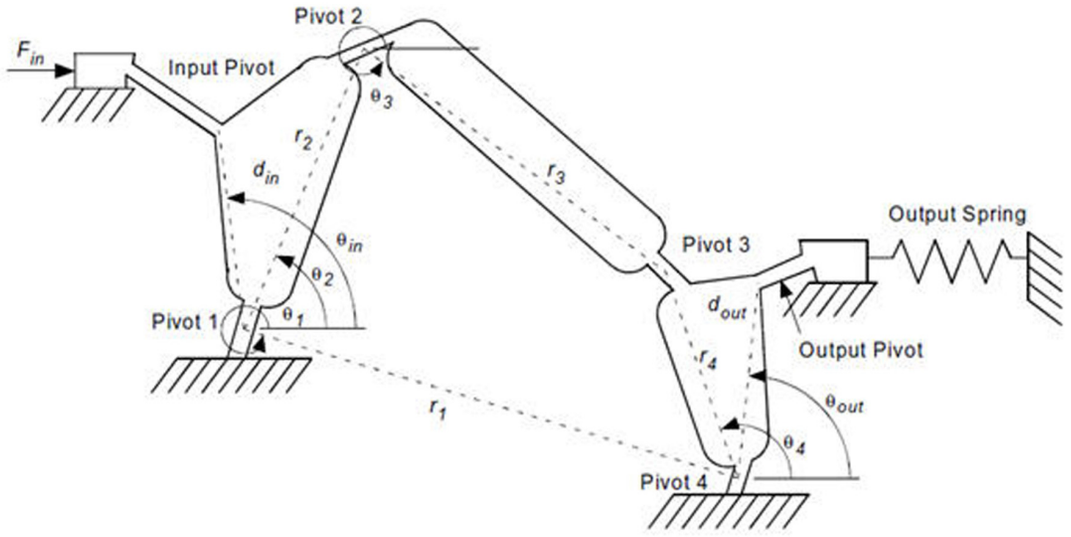

Figure 1. Schematic view of force or displacement amplifier' mechanism

Compliant MEMS have been used as a force amplifier in micro actuators and micro-mechanisms (Parkinson et al, 2001).

They are preferred since there is no need for assembly, no energy loss due to absence of friction, thus requiring no need for lubrication all of which providing high precision (Kosa et al, 2010). Besides, compliant micro mechanisms could be activated by mechanically (Han et al, 2007; Krishnan & Ananthasuresh, 2008), electro statically (Français et al, 2005; Millet et al, 2004), thermally (Lai et al, 2004; Terre & Shkel, 2004) or electrical (Gomm et al, 2002; Huang & Lan, 2006) induced forces.

Moreover, compliant MEMS having two or three clear stable states as named bi-stable or tri-stable behavior respectively were used in micro valve, micro switch, micro clasps applications (Chen et al, 2009; Jensen et al, 2001; Jensen & Howell, 2003; Nathan & Howell, 2003; Wilcox & Howell, 2005). For instance, Jensen designed several mechanisms such as double slider crank, slider-rocker mechanisms and explained the theory of bi-stable behavior (Jensen et al, 2004).

Recent studies on compliant mechanisms are focused on novel designs (Kosa et al, 2010), new developed methodologies and optimization in topology (Chour & Jyhjei, 2006; Krishnan & Ananthasuresh, 2008; Pedersen & Seshia, 2004), size and shape (Krishnan & Ananthasuresh, 2008) or the use of finite element methods (Jensen et al, 2001). Compliant micro mechanisms enable mechanical or geometric benefit meaning that the ratio of output force to input force and the ratio of output displacement to input displacement, respectively, and both mechanical and geometric advantage (MA and GA, respectively) are formulized as follows;

$$MA=F_{out}/F_{in} \quad (1)$$

$$GA=d_{out}/d_{in} \quad (2)$$

The energy is conserved during the motion transfer of compliant micro mechanism indicating that the increase in the output force causes decrease in the output displacement and vice versa. So, both mechanical and geometric benefits are significant to provide input to the micro actuators in MEMS applications (Kosa et al, 2010).

Optimization of compliant mechanisms such as topology and size optimization is a challenging issue. In topology optimization, it is critical to design a suitable functional configuration of the mechanism to provide desired output motion under applied forces while in size optimization, it is important to achieve desired force or displacement amplification so as to operate under maximum loads (Kota et al, 2001).

In this study, novel compliant MEMS force amplifier is designed and simulated by modeling its rigid body mechanism by Matlab/Simulink to determine the dynamic and quasi-static behavior. Kinematic approach is investigated and kinematic equations are derived and velocity and acceleration analysis of the micro mechanism are modeled. Dynamic response of MEMS amplifier is validated at a constant angular velocity and it is concluded that force amplification reaches to infinity at zero-crank angle. It is achieved that force amplification ratio reaches 5093, as the first stage crank angle, Θ_2 passes from 0° in quasi-static simulation.

2. Mechanism design

Compliant MEMS force amplifier's configuration is schematically shown in Fig. 2. Micro amplifier is composed of two slider-crank mechanisms. The two stage slider-crank amplifier provides force amplifying by means of its novel design. Its aim is to perform high output force at point B under low input forces. Two stages provide much more amplification compare to one stage. For both stages, rigid beams are linked by single thin flexible beams having a width of 3 μm. These flexible beams make the micro mechanism motion possible under operating forces. The micro mechanism stores energy and transfers force by elastic deformation of flexible beams linking rigid beams as both stage-slider cranks get close zero degree crank angle. Afterwards, input force is removed and micro amplifier springs back to its original position by means of flexible links having large deflections.

The beams in first stage have a length of 100 μm and width of 25 μm as the beams in second stage have a length of 800 μm and width of 25 μm, as all beams have rectangular cross sectional area. The depths of all beams are chosen as 25μm limited by SOI-MUMPs (Silicon on Insulator Multi User MEMS Process) manufacturing technology (Cohen et al, 2009).

2.1. Grashof theorem

In rigid body model of the MEMS amplifier, four-bar configuration is attained after vector loop equations are derived. Grashof theorem becomes significant to demonstrate the act of micro mechanism. Grashof theorem takes three cases into consideration and states that when both of beams are rocked it is called a double-rocker when both of beams are able to revolve, then it is called double-crank, when the short beam is able to rotate as the long one

is rocked, then it is called a crank-rocker mechanism. To determine the moving limit of the micro mechanism, the relation between the lengths of beams turns out to be an important issue. Therefore, selecting the length of a beam plays a crucial role for the micro mechanism.

Due the fact that, x1, x2 are assumed as length of the shortest beam and length of the longest beam, respectively, as x3, x4 are the mean lengths of the beams. If x1+x2<= x3+x4, at least one of the beams can rotate and If x1+x2= x3+x4, the mechanism is activated and crank has limited rotation this feature enables beams to pass horizontal positions closely to each other achieving a high force amplifying.

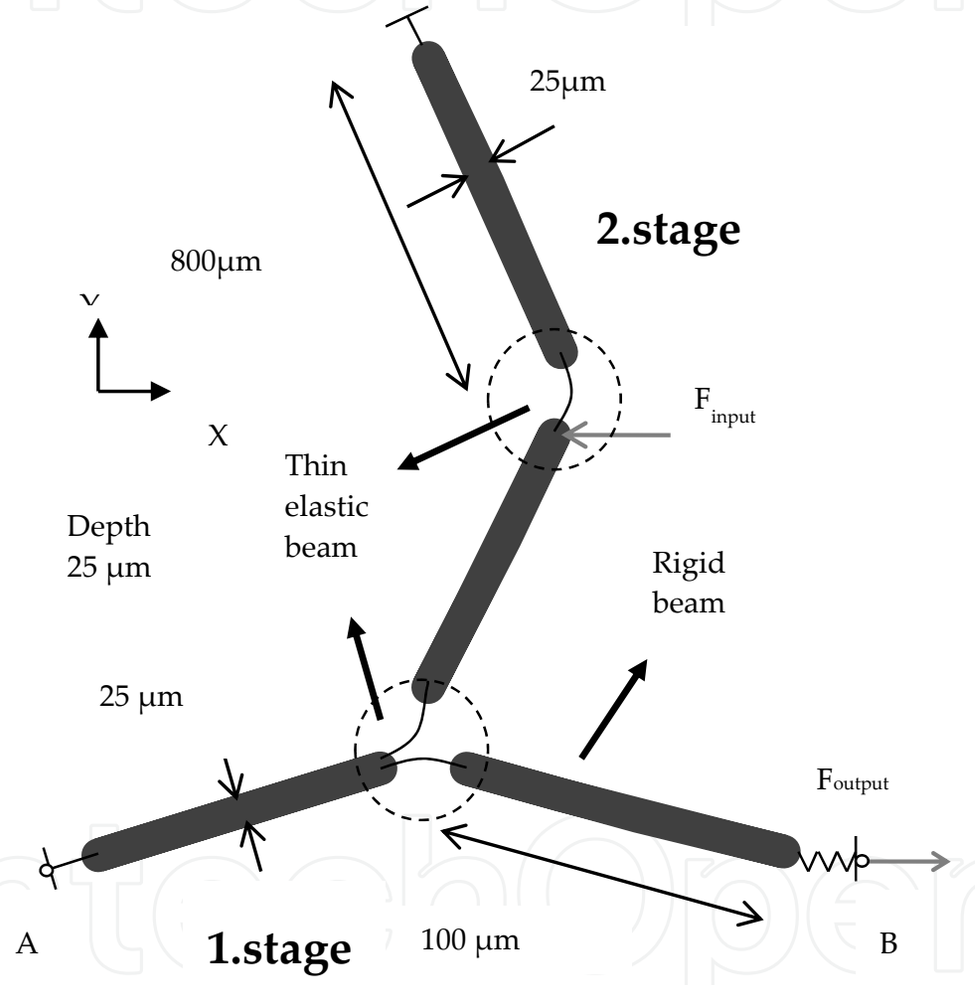

Figure 2. Novel compliant MEMS Force Amplifier

3. Analysis of quasi-static behavior

3.1. Force and moment equation derivation

Rigid body model of the compliant micro mechanism is considered. Free body diagram of each beam is sketched and a typical beam model is schematically shown in Fig. 3. Forces acting on each beam is broken down into x and y components as follows;

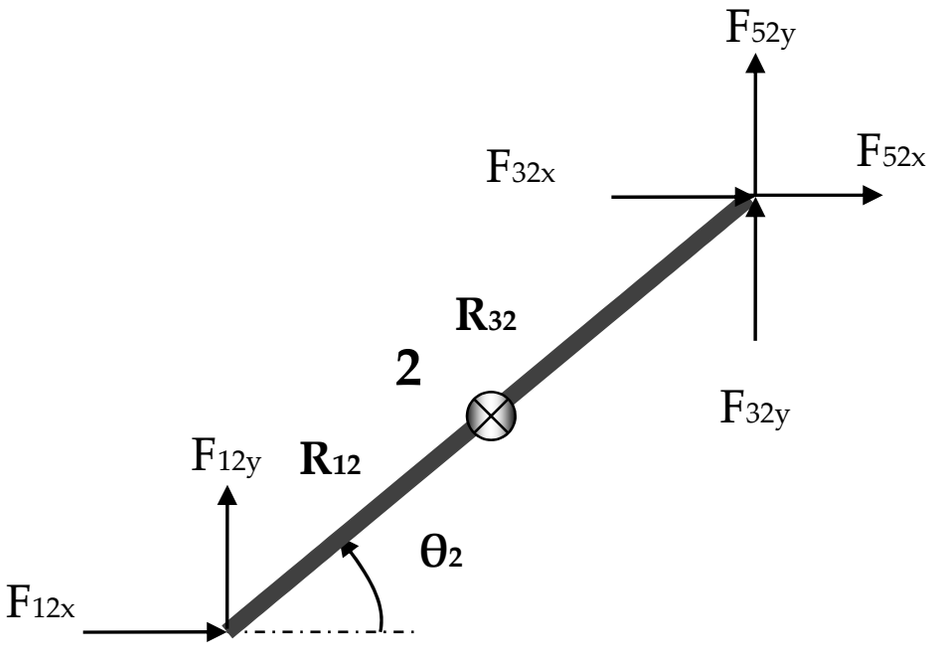

Figure 3. Free body diagram of beam 2

The static force and moment equations of beam 2 is typically shown and derived as; Equation derivation of forces acting on beam 2 along x axis;

$$\sum F_x = 0 \tag{3}$$

$$F_{12x} + F_{32x} + F_{52x} = 0 \tag{4}$$

Equation derivation of forces acting on beam 2 along y axis;

$$\sum F_y = 0 \tag{5}$$

$$F_{12y} + F_{32y} + F_{52y} = 0 \tag{6}$$

Equation derivation of moments acting on beam 2 along z axis;

$$\sum M_z = 0 \tag{7}$$

$$R_{12x} * F_{12y} - R_{12y} * F_{12x} + R_{32x} * F_{32y} - R_{32y} * F_{32x} + R_{52x} * F_{52y} - R_{52y} * F_{52x} = 0 \tag{8}$$

Free body diagram of beam 3 is shown in Fig. 4 and equation derivation of forces acting on beam 3 along x axis;

$$\sum F_x = 0 \tag{9}$$

$$F_{23x} + F_{43x} = 0 \tag{10}$$

Equation derivation of forces acting on beam 3 along y axis;

$$\sum F_y = 0 \tag{11}$$

$$F_{23y} + F_{43y} = 0 \tag{12}$$

Equation derivation of moments acting on beam 3 along z axis;

$$\sum M_z = 0 \tag{13}$$

$$R_{23x} * F_{23y} - R_{23y} * F_{23x} + R_{43x} * F_{43y} - R_{43y} * F_{43x} = 0 \tag{14}$$

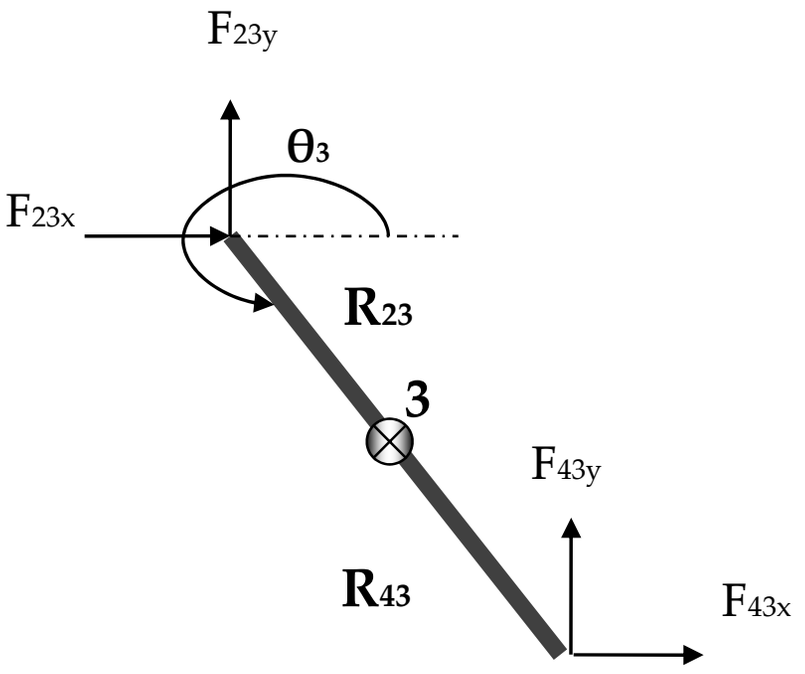

Figure 4. Free body diagram of beam 3

Free body diagram of beam 5 is shown in Fig. 5 and equation derivation of forces acting on beam 5 along x axis;

$$\sum F_x = 0 \tag{15}$$

$$F_{65x} + F_{25x} = 0 \tag{16}$$

Equation derivation of forces acting on beam 5 along y axis;

$$\sum F_y = 0 \tag{17}$$

$$F_{65y} + F_{25y} = 0 \tag{18}$$

Equation derivation of moments acting on beam 5 along z axis;

$$\sum M_z = 0 \tag{19}$$

$$R_{65x} * F_{65y} - R_{65y} * F_{65x} + R_{25x} * F_{25y} - R_{25y} * F_{25x} = 0 \tag{20}$$

Free body diagram of beam 6 is shown in Fig. 6 and equation derivation of forces acting on beam 6 along x axis;

$$\sum F_x = 0 \tag{21}$$

$$F_{g6x} + F_{56x} = 0 \tag{22}$$

Equation derivation of forces acting on beam 6 along y axis;

$$\sum F_y = 0 \tag{23}$$

$$F_{g6y} + F_{56y} = 0 \tag{24}$$

Equation derivation of moments acting on beam 6 along z axis;

$$\sum M_z = 0 \tag{25}$$

$$R_{g6x} * F_{g6y} - R_{g6y} * F_{g6x} + R_{56x} * F_{56y} - R_{56y} * F_{56x} = 0 \tag{26}$$

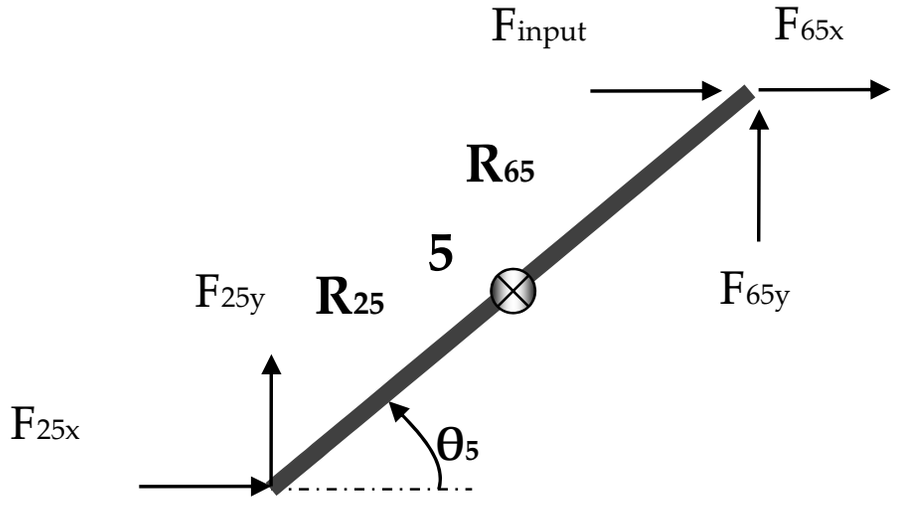

Figure 5. Free body diagram of beam 5

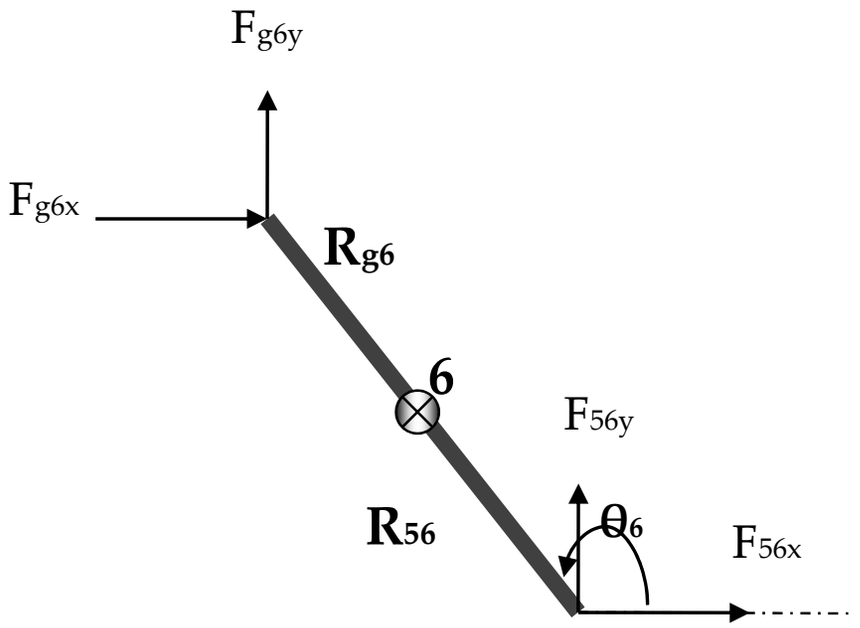

Figure 6. Free body diagram of beam 6

Free body diagram of slider is shown in Fig. 7 and equation derivation of forces acting on slider along x- and y- axes;

$$\sum F_x = 0 \tag{27}$$

$$F_{output} + F_{34x} = 0 \tag{28}$$

$$\sum F_y = 0 \tag{29}$$

$$F_{s4y} + F_{34y} = 0 \tag{30}$$

Thus, 14 force and moment equations are derived. Equations of relation between internal forces of beams;

$$F_{32x} = F_{23x} \tag{31}$$

$$F_{32y} = F_{23y} \tag{32}$$

$$F_{43x} = F_{34x} \tag{33}$$

$$F_{43y} = F_{34y} \tag{34}$$

$$F_{52x} = F_{25x} \tag{35}$$

$$F_{52y} = F_{25y} \tag{36}$$

$$F_{65x} = F_{56x} \tag{37}$$

$$F_{65y} = F_{56y} \tag{38}$$

8 equations are derived from the relations between internal forces of beams.

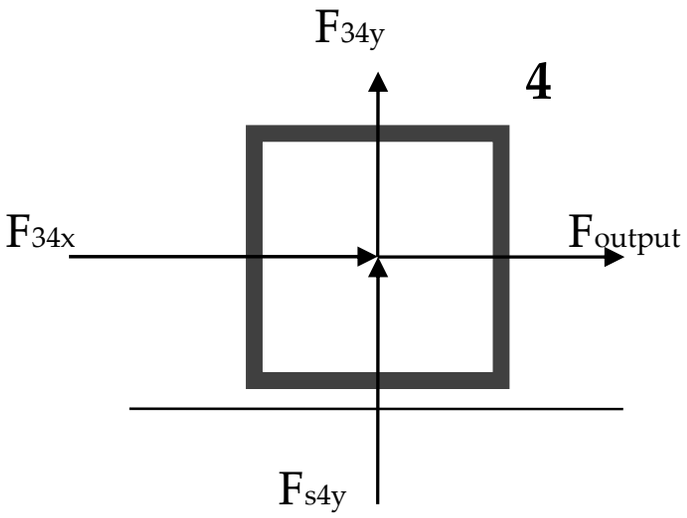

Figure 7. Free body diagram of slider

3.2. Equations and initial conditions

The vector loop equations are derived and broken down into x and y components as force and moment equations. It is seen that linear matrix method could not be used to solve the position problem. To analyze the position behavior of the micro mechanism, nonlinear and transcendental equations should be solved by Matlab and in quasi-static run, initial conditions of Θ_2 and (Θ_6-90°) are chosen as 10° and 20°, respectively.

3.3. Position analysis

The micro mechanism is a single degree of freedom mechanism and position analysis provides to inform the positions of other links and points as one of the links moves or rotates.

To find out position problem of the micro mechanism, nonlinear and transcendental vector loop equations that are derived and solved.

The vector loops are schematically shown in Fig. 8. There are two vector loop equations such as;

First vector loop equation:

$$R_2 + R_3 = R_1 \tag{39}$$

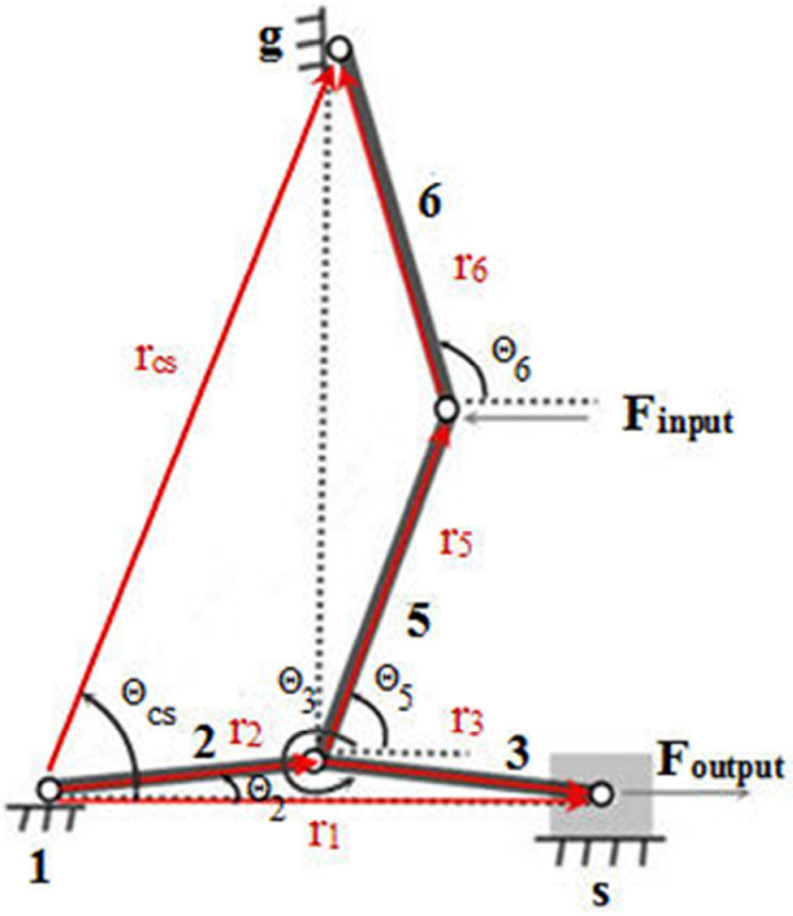

Figure 8. Vector loops for the force amplifier

Deriving equations according to coordinates of x and y:

$$r_2 * \cos\theta_2 + r_3 * \cos\theta_3 = r_1 \tag{40}$$

$$-r_2 * \sin\theta_2 - r_3 * \sin\theta_3 = 0 \tag{41}$$

Second vector loop equation:

$$R_2 + R_5 + R_6 = R_{cs} \tag{42}$$

Vector loop equations along x--axis

$$r_2 * \cos\theta_2 + r_5 * \cos\theta_5 + r_6 * \cos\theta_6 = r_{cs} * \cos\theta_{cs} \tag{43}$$

Vector loop equations along y--axis

$$r_2 * \sin\theta_2 + r_5 * \sin\theta_5 + r_6 * \sin\theta_6 = r_{cs} * \sin\theta_{cs} \tag{44}$$

By quasi-static analysis, it is claimed that (360°-Θ_3) and Θ_2 decreases linearly and are equal to each other during both quasi-static and dynamic simulations run by Matlab/Simulink. As seen in Fig. 9, it is calculated that as Θ_5 goes from 70° to 74.0248°, Θ_6 reduces from 110° to

105.9756°. Thus, as Θ_2 rotates 20°, both Θ_5 and Θ_2 rotates approximately 4.02° and slightly different from each other. The relation both between Θ_5 and Θ_2, Θ_6 and Θ_2 are linear.

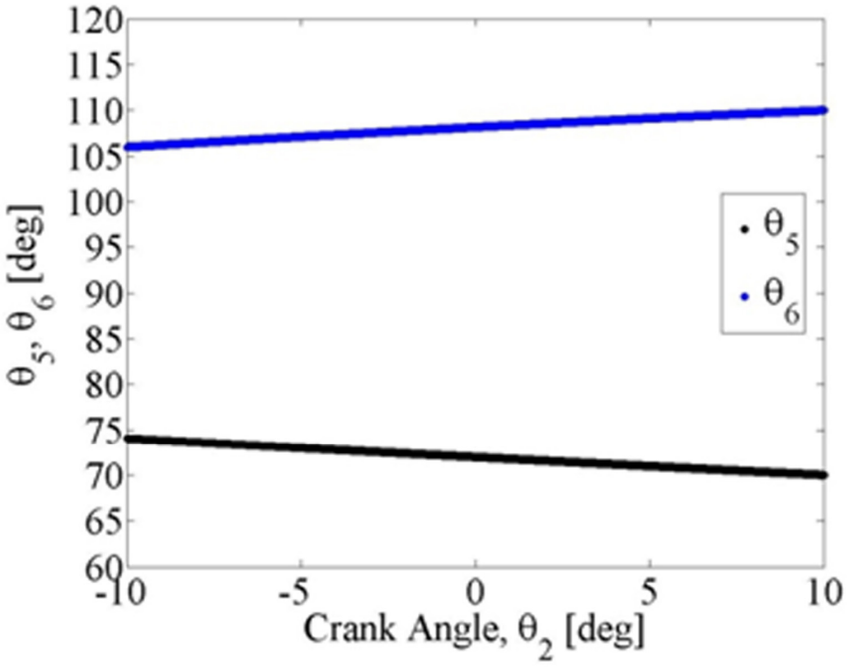

Figure 9. Plot of Θ_5 and Θ_6 according to first stage crank angle, Θ_2

Displacement ratio is defined as U_{output}/U_{input}. As the micro mechanism operates under an input force along – x direction, the first stage crank angle starts decreasing and pass from 0° and again starts increasing in an opposite direction and the ratio of output displacement to input displacement decreases as shown in Fig. 10. Beams 5 and 6 moves along –x and –y directions and the length of beams 5 and 6 are 8 times of beams 2 and 3. So, the input displacement increases rapidly than output displacement at close to zero degree crank angles. At negative crank angle values defining opposite directions, the slider gets close to initial position on contrast, beams 5 and 6 continue to get close to their vertical positions meaning that input displacement goes on to increase whereas output displacement begin to decrease. Therefore, after zero-crank angle, the displacement ratio continues to decrease according to Θ_2.

As the micro mechanism displays, both the second stage crank angle, (Θ_6-90°) and the first stage crank angle, Θ_2 get close to zero degree, the force amplification defined as F_{output}/F_{input} starts increasing and when Θ_2 is 0° and (Θ_6-90°) is at about small values, the micro mechanism provides high output force and force amplifying sharply increases as seen in Fig. 11 under $1.7*10^{-7}$ in [N]. Also, there are two peaks in force amplification by quasi-static run. As, the first crank angle is close to zero but at still positive value, the force amplifying reaches 5093 and after that step first crank angle gets negative value but it is still close to zero, the force amplification ratio is 4830 at negative direction due to the fact that the slider motion begin to move in opposite direction and also, output force is in opposite direction. It

is claimed that the toggle position of the micro mechanism is a very crucial issue meaning that if the initial conditions such as crank angles are adjusted properly to enable both crank angle pass 0° at the same time, the ratio of the output to the input force applied to the mechanism goes to infinity at zero degree crank angles.

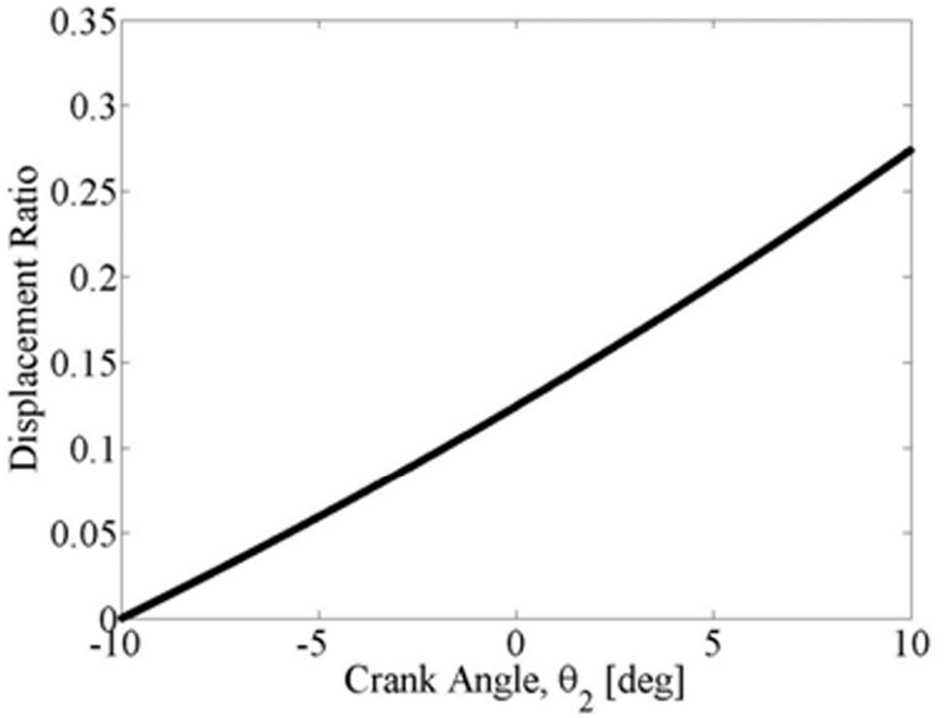

Figure 10. Plot of displacement ratio according to first stage crank angle, Θ_2

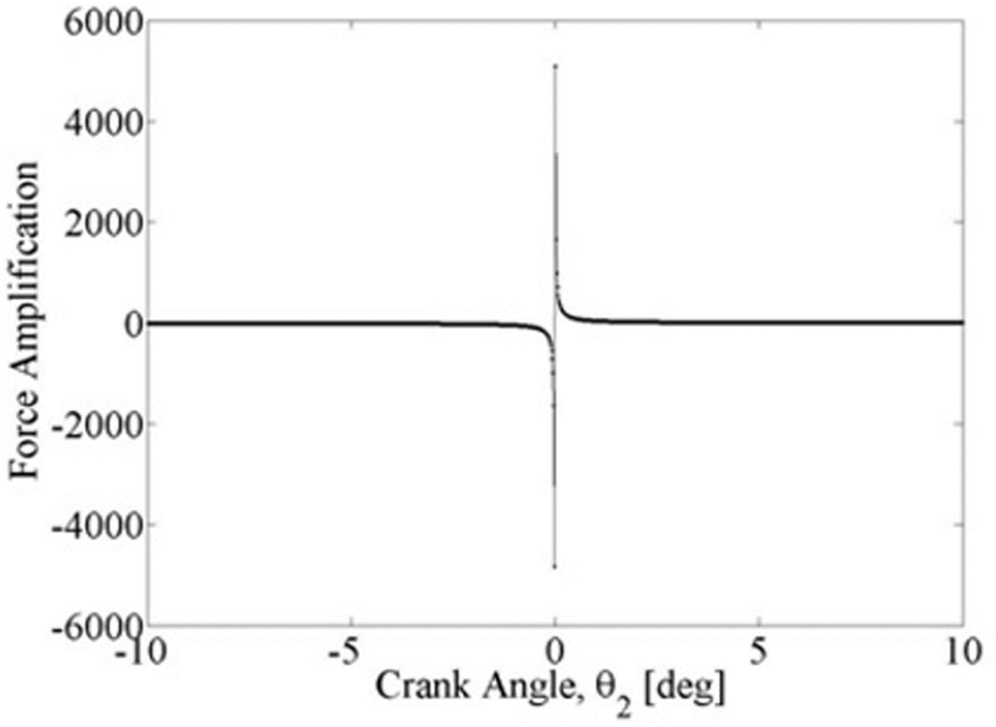

Figure 11. Plot of force amplifying according to first stage crank angle, Θ_2

4. Dynamic behavior of a novel MEMS amplifier

4.1. Inertial and geometric parameters:

It is assumed that micro mechanism is made up of silicon having a density of 2.33 g/cm^3. For short length of beams, lengths are 100 micron, widths and heights are 25 micron. The mass of short beams is;

$$M_s=2.33*100*25*25*10^{-15}=145625*10^{-18}\ [kg] \quad (45)$$

For long length of beams, lengths are 800 micron, widths and heights are 25 micron. The mass of short beams is;

$$M_l=2.33*800*25*25*10^{-15}=1165000*10^{-18}\ [kg] \quad (46)$$

The mass of the slider is accepted as $145625*10^{-18}$ in kilograms.

The mass moments of inertia of the beams are calculated as follows;

For short beams;

$$I_s = M_s *(L^2+a^2)/12=145625*10^{-18}*(100^2+25^2)/12=128938802.1*10^{-18}\ [kg*\mu m^2] \quad (47)$$

For long beams;

$$I_l = M_s *(L^2+a^2)/12=1165000*10^{-18} *(800^2+25^2)/12=6.219401042*10^{-8}[kg*\mu m^2] \quad (48)$$

4.2. Kinematic behavior

4.2.1. Velocity analysis

Kinematic simulation is used to calculate and to plot the velocities and acceleration of the beam of the MEMS amplifier.

To understand kinematic behavior of the mechanism, first of all, derivatives of vector loop equations derived in position analysis are taken with respect to time and the velocity equations are arranged as follows;

$$-r_2 * \sin\theta_2 * w_2 - r_3 * \sin\theta_3 * w_3 = \dot{r}_1 \quad (49)$$

$$r_2 * \cos\theta_2 * w_2 + r_3 * \cos\theta_3 * w_3 = 0 \quad (50)$$

$$-r_2 * \sin\theta_2 * w_2 - r_5 * \sin\theta_5 * w_5 - r_6 * \sin\theta_6 * w_6 = 0 \quad (51)$$

$$r_2 * \cos\theta_2 * w_2 + r_5 * \cos\theta_5 * w_5 + r_6 * \cos\theta_6 * w_6 = 0 \quad (52)$$

The beam 6 are rotated at a constant speed, 0.01 rad/s, in clockwise direction and the initial conditions of w_2, w_3, w_5, $\dot{r}_1$ are -0.059378175917485 [rad/s], 0.059378175917485 [rad/s], 0.011371580426033 [rad/s], 2.062182408251533 [μm/s], respectively.

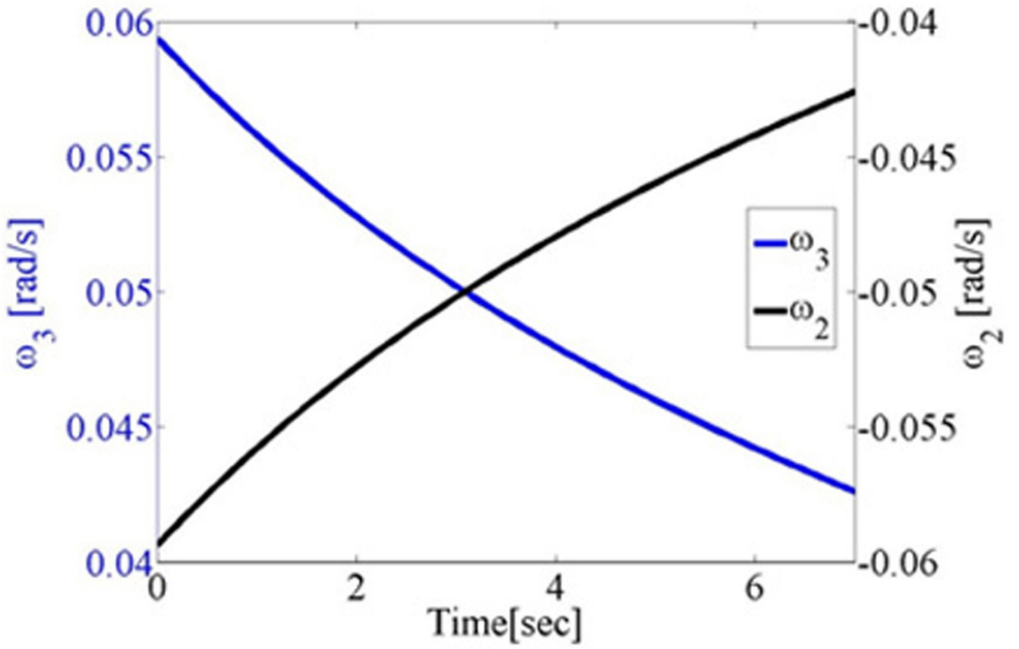

Figure 12. Plot of angular velocity of beam 2 and beam 3 versus time for simulation of force amplifier

The angular velocities of beams 2 and 3 in 1 stage are equal to each other in magnitude. As w_3 rotate counter clockwise direction, w_2 rotate clockwise direction and the absolute values of the changes in w_3 and w_2 equal to each other according to time as shown in Fig. 12.

Slider slows down until the first stage crank angle, Θ_2 pass from 0°. When first stage beams are fully open, as having horizontal position, slider velocity is equal to zero. Then the slider moves to along -x direction and angular velocity of beam 5 decreases according to time as in Fig. 13.

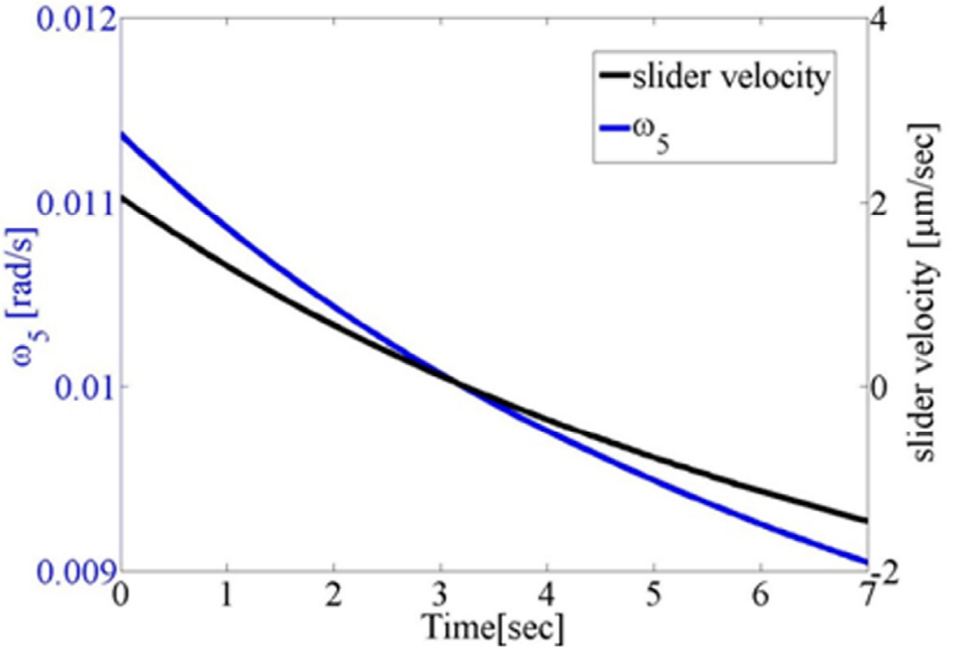

Figure 13. Plot of angular velocity of beam 5 and slider velocity versus time for simulation of force amplifier

4.2.2. Acceleration analysis

To analyze the acceleration of the beams, second derivatives of the terms must be handled. The second derivatives of the vector loop equations for the micro mechanism are as follows;

$$-r_2 * \cos\theta_2 * w_2^2 - r_2 * \sin\theta_2 * \alpha_2 - r_3 * \cos\theta_3 * w_3^2 - r_3 * \sin\theta_3 * \alpha_3 - \ddot{r}_1 = 0 \tag{53}$$

$$-r_2 * \sin\theta_2 * w_2^2 + r_2 * \cos\theta_2 * \alpha_2 - r_3 * \sin\theta_3 * w_3^2 + r_3 * \cos\theta_3 * \alpha_3 = 0 \tag{54}$$

$$\begin{aligned} &-r_2 * \cos\theta_2 * w_2^2 - r_2 * \sin\theta_2 * \alpha_2 - r_5 * \cos\theta_5 * w_5^2 \\ &-r_5 * \sin\theta_5 * \alpha_5 - r_6 * \cos\theta_6 * w_6^2 - r_6 * \sin\theta_6 * \alpha_6 = 0 \end{aligned} \tag{55}$$

$$\begin{aligned} &-r_2 * \sin\theta_2 * w_2^2 + r_2 * \cos\theta_2 * \alpha_2 - r_5 * \sin\theta_5 * w_5^2 \\ &+r_5 * \cos\theta_5 * \alpha_5 - r_6 * \sin\theta_6 * w_6^2 - r_6 * \cos\theta_6 * \alpha_6 = 0 \end{aligned} \tag{56}$$

In acceleration simulation by Simulink, the velocities such as w_2, w_3, w_5, $\dot{r}_1$, w_6 are considered as known. The beam 6 rotates at a constant speed meaning that acceleration of beam 6 is zero.

Acceleration of beam 2 and beam 3 are shown in fig. 14. Both acceleration of beams decrease as the micro mechanism operates under constant w_6, angular velocity. The magnitude of acceleration of beam 2 and beam 3 are equal to each other during simulation. Also, as seen in Fig. 15, acceleration of beam 5 and slider decrease as function of time.

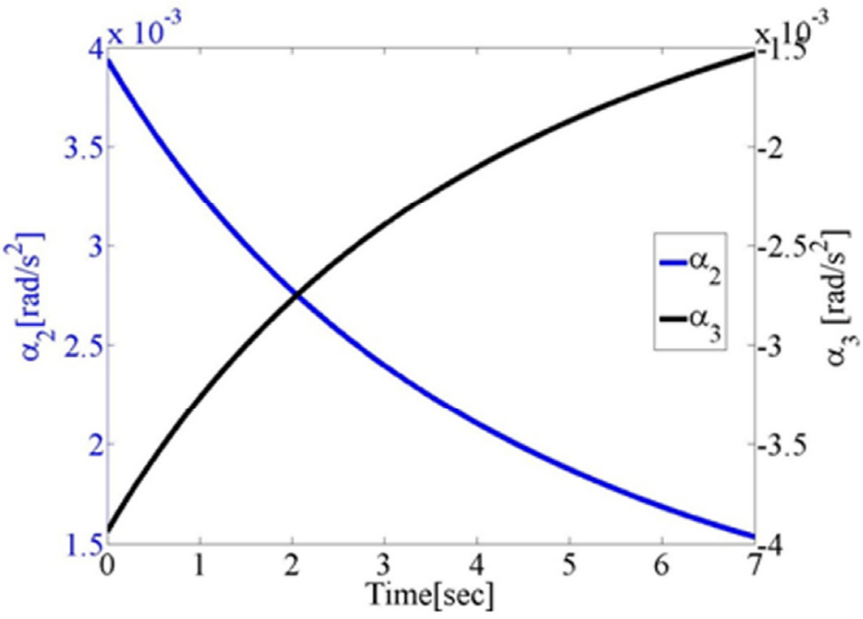

Figure 14. Acceleration of beam 2 and beam 3 under constant angular acceleration, α_2

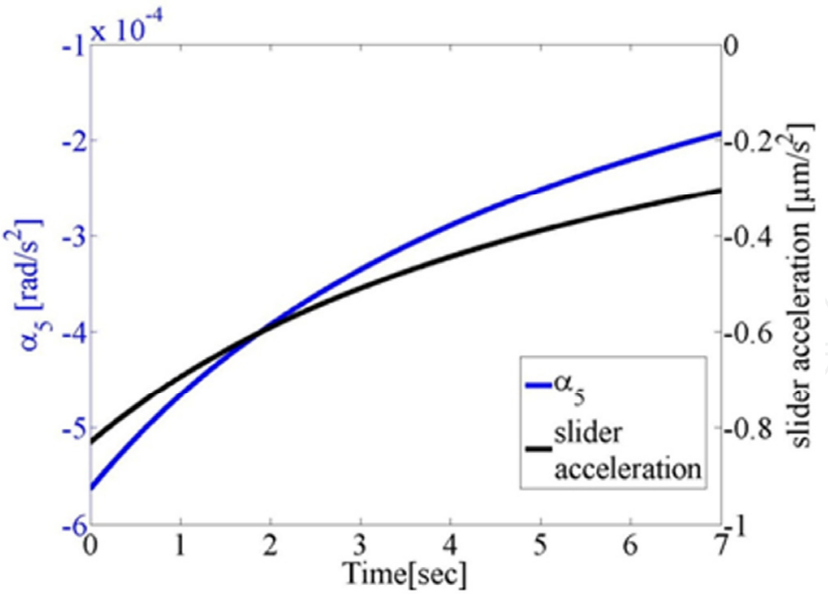

Figure 15. Acceleration of beam 5 and slider under constant angular acceleration, α_2

4.3. Acceleration vector equations according to center of mass

The linear acceleration of the center of mass equations are not present in vector loop equations that are previously derived. So, there must be equations relating to the acceleration of the center of mass of beams. Equation derivation is as follows and schematic representation of the center of mass acceleration in first and second loops is shown in Fig. 16 and Fig. 17, respectively.

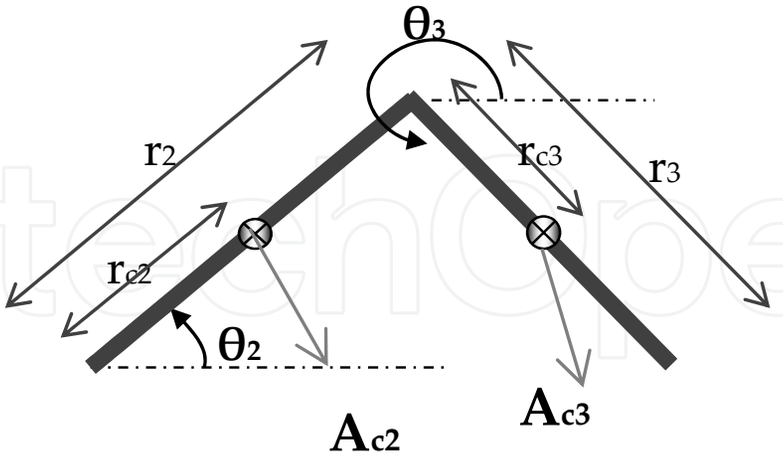

Figure 16. The center of mass acceleration in first loop

The center of mass acceleration of beam 2 along x and y direction;

$$A_{c2} = \ddot{R}_{c2} \tag{57}$$

$$A_{c2x} = -r_{c2} * \sin\theta_2 * \alpha_2 - r_{c2} * \cos\theta_2 * w_2^2 \tag{58}$$

$$A_{c2y} = r_{c2} * \cos\theta_2 * \alpha_2 - r_{c2} * \sin\theta_2 * w_2^2 \tag{59}$$

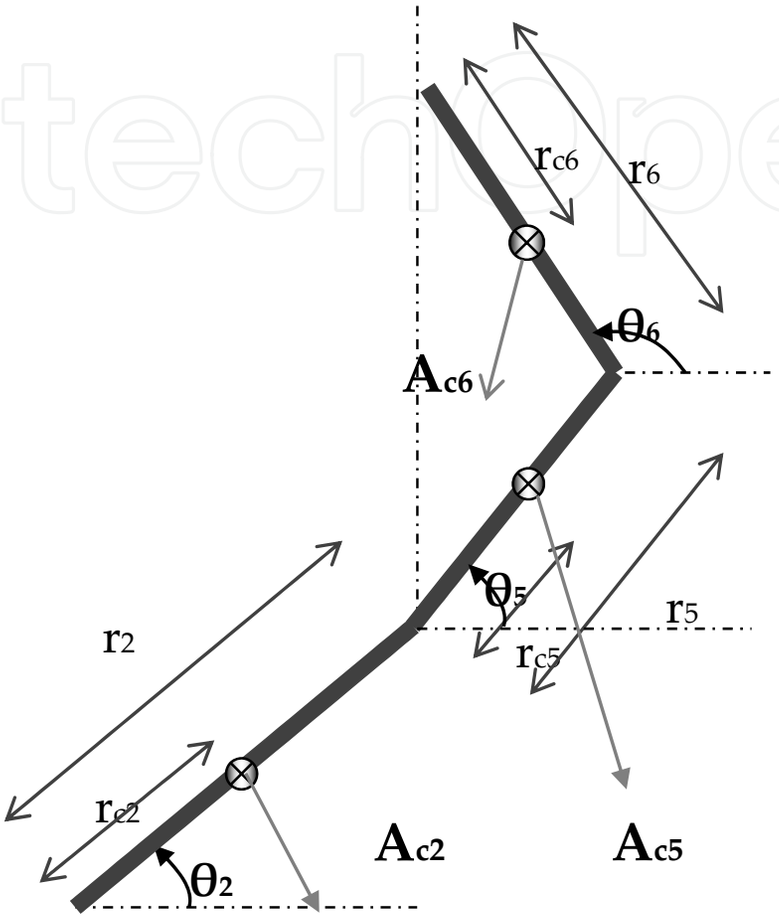

Figure 17. The center of mass acceleration in second loop

The center of mass acceleration of beam 3 along x and y direction;

$$A_{c3} = \ddot{R}_2 + \ddot{R}_{c3} \tag{60}$$

$$A_{c3x} = -r_2 * \sin\theta_2 * \alpha_2 - r_{c2} * \cos\theta_2 * w_2^2 - r_{c3} * \sin\theta_3 * \alpha_3 - r_{c3} * \cos\theta_3 * w_3^2 \tag{61}$$

$$A_{c3y} = r_2 * \cos\theta_2 * \alpha_2 - r_{c2} * \sin\theta_2 * w_2^2 + r_{c3} * \cos\theta_3 * \alpha_3 - r_{c3} * \sin\theta_3 * w_3^2 \tag{62}$$

The center of mass acceleration of beam 6 along x and y direction;

$$A_{c6} = \ddot{R}_{c6} \tag{63}$$

$$A_{c6y} = r_{c6} * \sin\theta_6 * \alpha_6 + r_{c6} * \cos\theta_6 * w_6^2 \tag{64}$$

$$A_{c6x} = -r_{c6} * \cos\theta_6 * \alpha_6 + r_{c6} * \sin\theta_6 * w_6^2 \tag{65}$$

The center of mass acceleration of beam 5 along x and y direction;

$$A_{c5} = \ddot{R}_2 + \ddot{R}_{c5} \tag{66}$$

$$A_{c5y} = r_6 * \sin\theta_6 * \alpha_6 + r_6 * \cos\theta_6 * w_6^2 + r_{c5} * \sin\theta_5 * \alpha_5 + r_{c5} * \cos\theta_5 * w_5^2 \tag{67}$$

$$A_{c5x} = -r_6 * \cos\theta_6 * \alpha_6 + r_6 * \sin\theta_2 * w_2^2 - r_{c5} * \cos\theta_5 * \alpha_5 - r_{c5} * \sin\theta_5 * w_5^2 \tag{68}$$

4.4. Force and dynamic analysis of the micro mechanism

The micro mechanism operates under constant angular velocity, 0.01 [rad/s], the slider crank starts increasing and reaches to its maximum value, 200 micron, meaning that the first stage slider crank is fully opened at 3.20 sec. then the first crank angle pass from 0° and slider begins to get close to its initial position and R_1 decreases as shown Fig. 18. According to both crank angles, Θ_2 and (90-Θ_6), the output force increases or decreases. In the first section of the F_{output} vs. time curve, first, both crank angles decrease, and two slider cranks start to open and at small crank angles, F_{output} sharply increase and at 3.20 sec Θ_2 is equal to 0.0013°

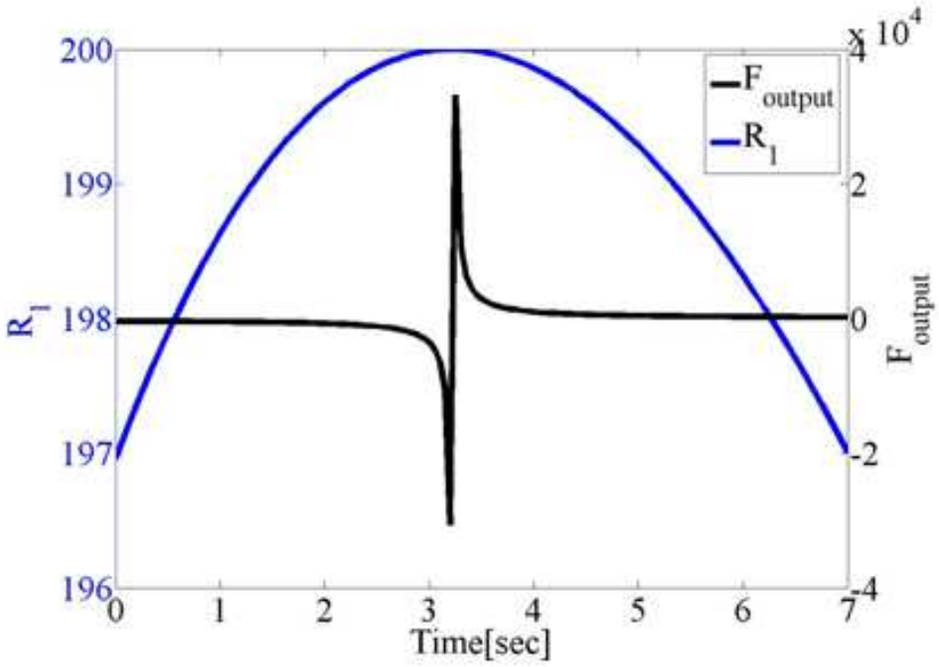

Figure 18. Displacement of slider and output force versus time

and at 3.25sec. Θ_2 is equal to -0.0012° and at Θ_2 these values, F_{output} goes to its peak values such as $-3.07*10^4$ μN at 3.20 sec. and $3.32*10^4$ μN at 3.25 sec. Θ_2 decreases until 3.20 sec. and then it increases, whereas 90°-Θ_6 decreases and gets close to small values during the simulation. The magnitude of first peak of F_{output} at 3.25 sec. is higher than the magnitude of second peak of F_{output} at 3.20 sec. due to the fact that (90°-Θ_6) at 3.25 sec. is smaller than the value of (90°-Θ_6) at 3.20 sec., meaning that small crank angle value of (90°-Θ_6) contributes to get much more output force.

5. Conclusion

The MEMS force amplifier designed in this study is shown to provide high output to input ratio.

By quasi-static analysis, 5090 force amplifying is achieved as the first crank angle, Θ_2, rotates 10° and passes from its horizontal position and (90°-Θ_6) rotates 1.85° and continues to decrease.

The maximum amplifying ratio changes based on the initial position of the micro mechanism. So, the toggle of the micro mechanism has a crucial role to get high force output and high force amplification. If the mechanism's initial position is adjusted properly as both crank angles pass 0° at the same time, the force output and consequently force amplification go to infinity.

If pseudo rigid body of the compliant MEMS force amplifier having elastic hinges is modeled as a further study, it would provide us to get much more close response to the micro mechanism's real behavior. This novel MEMS amplifier design achieves high force amplifying due to its geometric design.

By dynamic analysis, high output force is achieved as the micro mechanism operates under 0.01 [rad/s] constant angular velocity of beam 6 at 3.20 sec and at about fully open position of first crank angle.

By Simulink, the simulation displays dynamic behavior of the micro compliant mechanism and it is claimed that second stage crank angle rotates 4.01°, whereas first stage crank angle, Θ_2, rotates 19.92°.

5.1. Nomenclauture

R_1, r_1	vector of beam 1
R_2, r_2	vector of beam 2
R_3, r_3	vector of beam 3
R_5, r_5	vector of beam 5
R_6, r_6	vector of beam 6
R_{cs}, r_{cs}	vector of beam cs
F_{12x}	force of beam ground acting on link 2 along x direction
F_{12y}	force of beam ground acting on link 2 along y direction

F_{23x}	force of beam 2 acting on link 3 along x direction
F_{23y}	force of beam 2 acting on link 3 along y direction
F_{32x}	force of beam 3 acting on link 2 along x direction
F_{32y}	force of beam 3 acting on link 2 along y direction
F_{43x}	force of beam 4 acting on link 3 along x direction
F_{43y}	force of beam 4 acting on link 3 along y direction
F_{34x}	force of beam 3 acting on link 4 along x direction
F_{34y}	force of beam 3 acting on link 4 along y direction
F_{52x}	force of beam 5 acting on link 2 along x direction
F_{52y}	force of beam 5 acting on link 2 along y direction
F_{25x}	force of beam 2 acting on link 5 along x direction
F_{25y}	force of beam 2 acting on link 5 along y direction
F_{65x}	force of beam 6 acting on link 5 along x direction
F_{65y}	force of beam 6 acting on link 5 along y direction
F_{56x}	force of beam 5 acting on link 6 along x direction
F_{56y}	force of beam 5 acting on link 6 along y direction
F_{g6x}	force of ground acting on link 6 along x direction
F_{g6y}	force of ground acting on link 6 along y direction
A_{c2x}	center of mass acceleration of beam 2 along x direction
A_{c2y}	center of mass acceleration of beam 2 along y direction
A_{c3x}	center of mass acceleration of beam 3 along x direction
A_{c3y}	center of mass acceleration of beam 3 along y direction
A_{c5x}	center of mass acceleration of beam 5 along x direction
A_{c5y}	center of mass acceleration of beam 5 along y direction
A_{c6x}	center of mass acceleration of beam 6 along x direction
A_{c6y}	center of mass acceleration of beam 6 along y direction
α_2	angular acceleration of beam 2
α_3	angular acceleration of beam 3
α_5	angular acceleration of beam 5
α_6	angular acceleration of beam 6
F_{in}	input force
F_{out}	output force
M_z	moment acting on a beam along z axis
w_2	angular velocity of beam 2
w_3	angular velocity of beam 3
w_5	angular velocity of beam 5
w_6	angular velocity of beam 6
$\dot{R}_1, \dot{r}_1$	velocity of slider
$\ddot{R}_1, \ddot{r}_1$	acceleration of slider
Θ2	first stage crank angle
Θ3	angle of beam 3 from +x axis in counter clockwise direction
Θ5	angle of beam 5 from +x axis in counter clockwise direction
Θ6	angle of beam 6 from +x axis in counter clockwise direction

Author details

Ergin Kosa* and Levent Trabzon
Mechanical Engineering, Istanbul Technical University, Istanbul, Turkey

Umit Sonmez
Mechanical Engineering, Sharjah University, Dubai, United Arab Emirates

Huseyin Kizil
Metallurgical and Materials Engineering, Istanbul Technical University, Istanbul, Turkey

6. References

Ashok, M.; Howell, L. L. & Norton, T. W. (2000). Limit Positions of Compliant Mechanisms Using the Pseudo-Rigid-Body Model Concept. Mechanism and Machine Theory, Vol. 35, pp. 99-115

Chen, G.; Wilcox, D. L. & Howell L. L. (2009). Fully Compliant Double Tensural Tristable Micromechanisms (DTTM), *Journal of Micromechanics and Microengineering*, Vol., 19, pp. 1-8

Cohen, A.; Hames, G.; Monk, D., Wilcenski, S. & Hardy B. (2009). Soimumps Design Handbook, MEMSCAP Revision 5.

Français, O.; Rousseau, L., Bourouina, T., Haussy, J. & Tissot, A. (2005). MEMS Memory Based on Bi-stable Mechanical Structures, Proceedings of DTIP of MEMS and MOEMS, ISBN 2-84813-0357-1, Montreux, Switzerland, June, 2005

Gomm, T.; Howell, L. L. & Selfridge, R. H. (2002). In-plane Linear Displacement Bistable Microrelay, *Journal of Micromechanics and Microengineering*, Vol. 12, pp. 257–264

Han, J. S.; Müller, C., Wallrabe, U. & Korvink, J. G. (2007). Design, Simulation, and Fabrication of a Quadstable Monolithic Mechanism with *X*- and *Y*-Directional Bistable Curved Beams. *Journal of Mechanical Design*, Vol. 129, pp. 1198-2003

Hsu, Tai Ran. (2002). *MEMS & Microsystems Design and Manufacture*, McGraw Hill (1st edition), ISBN 0-07-113051, USA

Huang, S. C. & Lan, G. J. (2006). Design and Fabrication of a Micro Compliant Amplifier with a Topology Optimal Compliant Mechanism Integrated with a Piezoelectric Microactuator. *Journal of Micromechanics and Microengineering*, Vol. 16, pp. 531–538. ISSN 0960-1317

Jensen, B. D.; Parkinson, Matthew B., Kurabayashi, Katsuo, Howell, Larry L. & Baker, Michael S. (2001). Design Optimization of a Fully-Compliant Bistable Micromechanism, Proceedings of 2001 ASME International Mechanical Engineering Congress and Exposition, New York, November, 2001

Jensen, B. D. & Howell, L. L. (2003). Identification of Compliant Pseudo-Rigid-Body Four-Link Mechanism Configurations Resulting in Bistable Behavior. *Journal of Mechanical Design*, Vol. 125, pp. 701-708

* Corresponding Author

Jensen, B. D. & Howell, L. L. (2004). Bistable Configurations of Compliant Mechanisms Modeled Using Four Links and Translational Joints. *Journal of Mechanical Design*. Vol. 126 , pp. 657-666

Kosa, E.; Sonmez, U., Kizil, H. & Trabzon L. (2010). The Design and Analysis of a Novel MEMS Force Amplifier. *Turkish Journal of Engineering & Environmental Sciences*, Vol. 34, pp. 253–259

Kota, S.; Joo J., Li Z., Rodgers, S. M. & Sniegowski J. (2001). Design of Compliant Mechanisms: Applications to MEMS. *Analog Integrated Circuits and Signal Processing*, Vol. 29, pp. 7-15

Krishnan , G. & Ananthasuresh G. K. (2008). Evaluation and Design of Displacement-Amplifying Compliant Mechanisms for Sensor Applications. *Journal of Mechanical Design*, Vol. 130, pp. 1-9

Lai, Y.; McDonald , J., Kujath, M. & Hubbard, T., (2004). Force, Deflection and Power Measurements of Toggled Microthermal Actuators. *Journal of Micromechanics and Microengineering*, Vol. 14, pp. 49–56

Larry, H. L. (2001). *Compliant Mechanisms*, John Wiley & Sons, ISBN 0-471-38478-X, USA.

Li, J.; Liu, Z. S., Lu, C., Zhang, Q. X. & Liu, A. Q. (2005). A Self Limited Large Displacement Ratio Micromechanical Amplifier. *Proceedings of The 13th International Conference on Solid-State Sensors, Actuators and Microsystems*, ISBN 0-7803-8952-2, Seoul, Korea, June, 2005

Lobontiu, N.; Paine, J. S. N., Garcia, E. & Goldfarb, M. (2001). Corner-Filleted Flexure Hinges. *Journal of Mechanical Design*, Vol. 123, pp. 346-352

Millet, O.; Bernardoni, P., Régnier, S., Bidaud, P., Tsitsiris, E., Collard, Dominique. & Buchaillot, Lionel. (2004). Electrostatic Actuated Micro Gripper using an Amplification Mechanism, *Sensors and Actuators A*, Vol. 114, pp. 371–378

Nathan, D. & Howell, Larry L. (2003). A Self-Retracting Fully Compliant Bistable Micromechanism. *Journal of Microelectromechanical Systems*, Vol. 12, pp. 273-280

Parkinson, M. B.; Jensen, B. D. & Kurabayashi K. (2001). Design of Compliant Force and Displacement Amplification Micro-Mechanisms. *Proceedings of DETC'01 ASME, Design Engineering Technical Conferences and Computers and Information in Engineering Conference*, Pittsburgh, Pennsylvania, September, 2001

Pedersen, C. B. W. & Seshia, A. A. (2004). On the Optimization of Compliant Force Amplifier Mechanisms for Surface Micromachined Resonant Accelerometers. *Journal of Micromechanics and Microengineering*, Vol. 14, pp. 1281–1293

Sreekumar, M.; Nagarajan, T. & Singaperumal, M. (2008). Experimental Investigations of the Large Deflection Capabilities of a Compliant Parallel Mechanism Actuated by Shape Memory Alloy Wires. *Smart materials and structures,* Vol. 17, pp. 1-12

Tantanawat , T. & Kota, S. (2007). Design of Compliant Mechanisms for Minimizing Input Power in Dynamic Applications. *Journal of Mechanical Design*, Vol. 129, pp. 1064-1075

Terre, J. C. & Shkel, A. (2004). Dynamic Analysis of a Snap-Action Micromechanism, *IEEE*, pp. 1245-1248

Wilcox, D. L. & Howell, L. L. (2005). Fully Compliant Tensural Bistable Micromechanisms (FTBM). *Journal of Microelectromechanical Systems*, Vol. 14, pp. 1-8